Structural Basis for the Distinct Membrane Binding Activity of the Homologous C2A Domains of Myoferlin and Dysferlin

Faraz M. Harsini[1,2], Anthony A. Bui[3], Anne M. Rice[4], Sukanya Chebrolu[1], Kerry L. Fuson[1], Andrei Turtoi[5,6,7], Mazdak Bradberry[9], Edwin R. Chapman[8,9] and R. Bryan Sutton[1,2]

*1 - **Department of Cell Physiology and Molecular Biophysics,** Texas Tech University Health Sciences Center, Lubbock, TX, 79430, USA*
*2 - **Center for Membrane Protein Research,** Texas Tech University Health Sciences Center, Lubbock, TX, 79430, USA*
*3 - **Department of Chemistry and Biochemistry,** Texas Tech University, Lubbock, TX, 79409, USA*
*4 - **Department of Biophysics,** Johns Hopkins University, Baltimore, MD, 21205, USA*
*5 - **Tumor Microenvironment and Resistance to Treatment Lab,** Institut de Recherche en Cancrologie de Montpellier, 34090 Montpellier, France*
*6 - **Institut du Cancer Montpellier,** 34090 Montpellier, France*
*7 - **Universit Montpellier,** 34298 Montpellier, France*
*8 - **Howard Hughes Medical Institute,** University of Wisconsin-Madison, Madison, WI, 53705, USA*
*9 - **Department of Neuroscience,** University of Wisconsin-Madison, Madison, WI, 53705, USA*

Correspondence to R. Bryan Sutton: *roger.b.sutton@ttuhsc.edu*
https://doi.org/10.1016/j.jmb.2019.04.006
Edited by James Sellers

Abstract

Dysferlin has been implicated in acute membrane repair processes, whereas myoferlin's activity is maximal during the myoblast fusion stage of early skeletal muscle cell development. Both proteins are similar in size and domain structure; however, despite the overall similarity, myoferlin's known physiological functions do not overlap with those of dysferlin. Here we present for the first time the X-ray crystal structure of human myoferlin C2A to 1.9 Å resolution bound to two divalent cations, and compare its three-dimensional structure and membrane binding activities to that of dysferlin C2A. We find that while dysferlin C2A binds membranes in a Ca^{2+}-dependent manner, Ca^{2+} binding was the rate-limiting kinetic step for this interaction. Myoferlin C2A, on the other hand, binds two calcium ions with an affinity 3-fold lower than that of dysferlin C2A; and, surprisingly, myoferlin C2A binds only marginally to phospholipid mixtures with a high fraction of phosphatidylserine.

Introduction

The ability to modify and sculpt phospholipid membranes in a regulated manner is a critical process for almost all cell types. These processes involve the fusion of neurotransmitter-containing vesicles for cell-to-cell communication in the case of neurons, gene transfer in the case of viruses, and maintenance of membrane integrity in the case of membrane repair. Dysferlin (*DYSF*) is a 237-kDa type II integral membrane protein that facilitates the Ca^{2+}-dependent aspects of membrane repair. Dysferlin is expressed in all mammalian tissues, but a mutant phenotype is more prevalent in human skeletal muscle. Prolonged membrane damage stimulates a cascade of immune factors that ultimately results in extensive muscle inflammation and damage [1–3]. Failure to adequately repair this damage can result in a gradual and progressive loss of muscle tissue. Indeed, mutations in the *DYSF* gene have been linked to limb–girdle muscular dystrophy type 2B (LGMD-2B) or Miyoshi myopathy (MM) in humans [4]. Dysferlin rapidly responds to injury by sensing Ca^{2+} influx through the site of damage, and then facilitates Ca^{2+}-dependent patch-repair [5,6]. Dysferlin-deficient muscle fibers demonstrate a primary defect in Ca^{2+}-dependent, vesicle-mediated membrane repair [7]. Given the association of dysferlin with LGMD-2B and MM, and its importance in maintaining the integrity of the cell membrane, this protein has been hypothesized to play a critical role as a facilitator of membrane repair in skeletal muscles.

Myoferlin is a 230-kDa type II integral membrane protein that is encoded by the MYOF gene and is a paralog of dysferlin [8]. The protein is expressed in myoblasts, endothelial cells, and cardiac and skeletal muscles. Myoferlin expression can also be detected in pulmonary tissue and at very low levels in the kidney, placenta, and brain [9]. Myoferlin-null mice myoblasts are not able to form syncytial myotubes, and as a result, they cannot generate the large myofibers needed to form skeletal muscles [10]. Myoferlin mRNA is upregulated in patients diagnosed with Duchenne muscular dystrophy [11–13]. Indeed, increased levels of myoferlin measured in Duchenne muscular dystrophy patients suggest a role for myoferlin in muscle regeneration and muscle repair [10]. Aberrant myoferlin expression has also been linked to cancer progression, as the protein is overexpressed in numerous cancers (e.g., pancreas, lung, liver, breast, kidney) [14–18]. Its depletion results in impairment of caveole formation, perturbed EGFR and VEGFR2 activity, altered metabolism and mitochondrial function, reduced exosome formation and overall decrease of proliferative, migratory, and invasive properties of tumors [19–23].

The overall domain structure of both dysferlin and myoferlin is arranged as seven tandem C2 domains labeled C2A–C2G (Fig. 1A), a Ca^{2+}-dependent, membrane-binding four-helix bundle domain known as FerA [25], and a Trp–Arg-rich DysF domain [26]. Both dysferlin and myoferlin possess a single C-terminal transmembrane helix that is embedded within a patching vesicle. The multiple C2 motifs are the most characteristic features of the ferlin proteins. C2 domains are typically Ca^{2+}-dependent phospholipid binding domains with an approximate length of 130 amino acids [27]. Among all C2 domains of dysferlin, only the C2A domain strongly binds to lipids in a Ca^{2+}-dependent manner [28]. The other C2 domains show weaker or Ca^{2+}-independent binding to phospholipids [28,29]. In addition to C2A, C2E and C2F domains have been shown to play a core roll in the function of ferlin protein activity [30,31].

Although roles for dysferlin and myoferlin in normal maturation and function of muscle cells have been posited, a lack of knowledge about the characteristics and specific functions of the various domains of these proteins is a major obstacle in understanding their respective mechanism of action. The physiological differences between dysferlin and myoferlin are supported by the fact that, despite their overall similarity, they do not appear to be functionally interchangeable [32]. Our analysis of the C2A domains from both proteins shows that dysferlin C2A binds phospholipid in the presence of Ca^{2+} slower than other C2 domains. In addition, myoferlin binds Ca^{2+} with a much lower affinity than dysferlin C2A; and, its Ca^{2+}-dependent phospholipid-binding activity is much reduced relative to dysferlin C2A. These findings define crucial differences between myoferlin and dysferlin that may explain why these two paralogs cannot fully complement the function of the other.

Results

X-ray crystal structure of human myoferlin C2A

Human myoferlin C2A (residues 1–125) was crystallized in 0.1 M Bis–Tris (pH 6.5), 20% PEG 3350, 0.3 M $SrCl_2$, or $CaCl_2$. Strontium ion has been used as a surrogate for Ca^{2+} in many Ca^{2+}-binding proteins, including the C2B domain of synaptotagmin 1 [33]. We completed the Sr^{2+}-bound form for phasing purposes, which we did not utilize. Furthermore, the quality of the Sr^{2+}-bound crystals was better than the Ca^{2+}-bound form of myoferlin C2A crystals. The cell constants of the two data sets were almost identical. Crystals were grown at 23 ° C (Fig. 2A) in space group $P2_12_12_1$ with

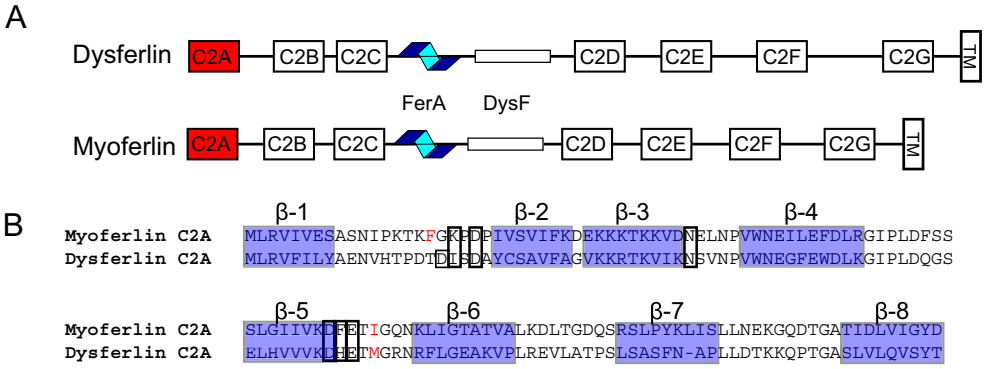

Fig. 1. (A) Domain schematic of the dysferlin and myoferlin proteins. C2 domains are shown as boxes, FerA is depicted as a helical cartoon. The domains highlighted in red are the two C2A domains under consideration. (B) Structure-based alignment of dysferlin C2A and myoferlin C2A [24]. β-Strands are labeled above and highlighted as blue-shaded boxes. Residues observed to coordinate Ca^{2+} are boxed. Hydrophobic residues at the Ca^{2+}-binding site that interact with the membrane are shown in red.

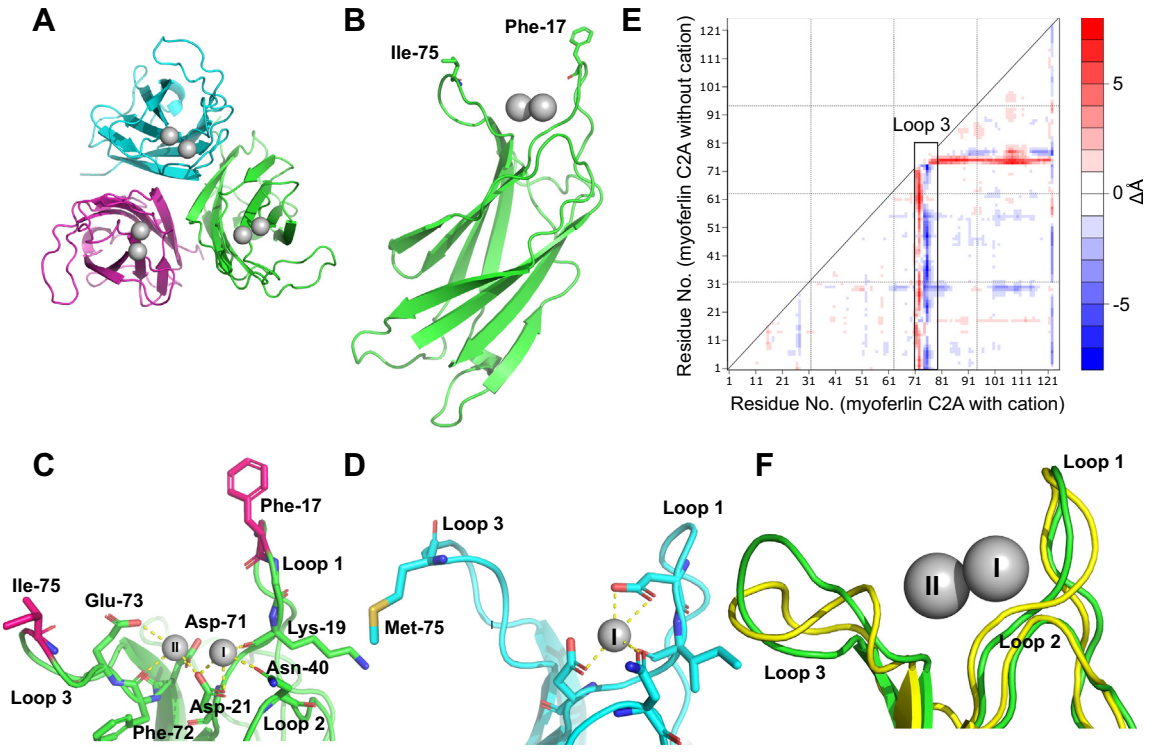

Fig. 2. (A) The asymmetric unit of human myoferlin C2A crystallized with Sr^{2+}. (B) Single myoferlin C2A domain highlighting Phe-17 and Ile-75 putative membrane-anchoring residues. (C) Close-up of Ca^{2+}-binding residues of myoferlin C2A. Calcium ion 'I' is analogous to the calcium ion found in dysferlin C2A bound to the high-affinity Ca^{2+}-binding pocket [34]. (D) Dysferlin C2A structure (chain E of PDB code: 4IHB) showing the single calcium ion observed in dysferlin C2A. The residues that make up the loops 1, 2, and 3 are shown as sticks. (E) Distance-difference matrix comparing liganded *versus* un-liganded myoferlin C2A. Loop 3 residues are boxed. (F) Superposition of myoferlin 2DMH (yellow, without divalent cation) and myoferlin from this X-ray crystal structure (green, with Sr^{2+}). Calcium ion binding loops are labeled.

three molecules in the asymmetric unit (Table 1). X-ray data were collected at Stanford Synchrotron Radiation Lightsource (SSRL). The crystals diffracted to 1.93 Å and were solved by molecular replacement (Fig. 2) using the NMR-derived structure of Ca^{2+}-free myoferlin C2A as the search model (2DMH [35]). Previously, we solved the crystal structures of dysferlin C2A and dysferlin C2Av1 (C2A variant 1) [34]. Both dysferlin C2A domains crystallized with three molecules in the asymmetric unit, and interestingly, the inner DysF domain of dysferlin also crystallized with three molecules in the asymmetric unit [26]. While it is tempting to speculate about the oligomerization state of ferlins based on crystallographic observations, currently there are no other experimental indications that implicates trimerization with ferlin function.

Myoferlin C2A consists of eight β-strands with a type-2 (P-type) C2 domain topology. The β-strands form three loops (loops 1, 2, and 3) at the apex of the C2 domain that shape the divalent binding pocket. In myoferlin C2A, loop 3 possesses three of the residues that bind Ca^{2+} (Asp-71, Phe-72, Glu-73). Loop 2 possesses one of the Ca^{2+}-binding residues (Asn-40) (sites I and II, Fig. 2C). The phospholipid-binding residues of C2 domains are typically linked to the same loops that bind Ca^{2+}. Phe-17 on loop 1 and Ile-75 on loop 3 (Fig. 2B and C) are located at the apex of their respective loops and should act as phospholipid-anchoring residues for this C2A domain (Fig. 2B) [36].

An NMR solution structure of the un-liganded human myoferlin C2A was initially deposited with the PDB by the RIKEN Structural Genomics/Proteomics Initiative as 2DMH in 2006 [35]. As such, no accompanying biochemical data were published. We can therefore compare the 20 NMR structures of the un-liganded myoferlin C2A domain with our ligand-bound x-ray structure of myoferlin C2A within the experimental limits of the two structures (RMSD of atomic positions = 0.96 ± 0.06 Å, overall Cα atoms). No Ca^{2+} or divalent cation was reported in the NMR structure of myoferlin C2A [35]. It is possible that the myoferlin C2A used for the NMR structure could have access to calcium ions from the buffer solution. However, the rotamers of the acidic residues coordinating the divalent cations in the crystal structure *versus* the solution-state structure are clearly different. Therefore, it is unlikely that the NMR structure contained bound divalent cations.

Table 1. Crystallographic summary of myoferlin C2A

Resolution range (Å)	41.14–1.93 (1.99–1.93)
Space group	$P2_12_12_1$
Unit cell (Å)	47.35, 83.11, 94.28
Total reflections	333,686 (32,892)
Unique reflections	28,689 (2825)
Multiplicity	11.6 (11.6)
Completeness (%)	99.52 (99.82)
Mean $I/\sigma(I)$	9.5 (1.7)
Wilson *B*-factor	20.0
R_{merge}	0.112 (0.645)
R_{meas}	0.135 (0.777)
R_{pim}	0.060 (0.348)
$CC_{1/2}$	0.907 (0.779)
Reflections used in refinement	28,580 (2825)
Reflections used for R_{free}	2793 (260)
R_{work}	0.181 (0.232)
R_{free}	0.192 (0.244)
Number of non-hydrogen atoms	3496
Ligands	6
Solvent	470
Protein residues	387
RMS (bonds, Å)	0.017
RMS (angles, °)	1.87
Ramachandran favored (%)	97.9
Ramachandran allowed (%)	2.1
Ramachandran outliers (%)	0
Rotamer outliers (%)	0
Clashscore	0.97
Average *B*-factor (Å^2)	29.00
Macromolecules (Å^2)	26.94
Ligands (Å^2)	30.82
solvent (Å^2)	31.89

The most obvious difference between the two structures is the deviation of loop 3 (Fig. 2E, F). The difference-distance matrix of myoferlin C2A without Ca^{2+} (2DMH) was subtracted from the difference-distance matrix of the crystal structure of myoferlin C2A with bound cations. A difference-distance matrix is generated by calculating the distances between all pairs of equivalent Cα atoms in each molecule and then subtracting those distances. This allows a means of quantitatively assessing any structural similarity or differences between two structures. (Fig. 2E). The residues that form loop 3 (residues 71–79) deviate significantly, indicating a significant difference between the two loops. Interestingly, there is little difference in the loop 1 (residues 12–22) conformation between unliganded and liganded structures of myoferlin C2A, thus suggesting an unusually rigid loop 1 structure (Fig. 2E, F).

Differences in Ca^{2+} binding between myoferlin C2A and dysferlin C2A

Despite the overall similarity between the three-dimensional structures of myoferlin and dysferlin C2A (RMSD = 1.91 Å, over all Cα atoms), the manner in which Ca^{2+} is coordinated between the two domains is different. Using the dysferlin C2A structure as a reference, the first Ca^{2+}-binding site in myoferlin C2A

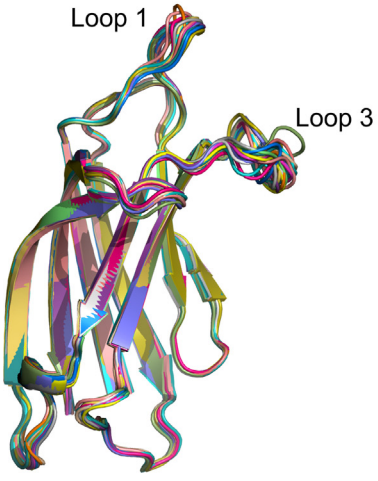

(a) NMR structures of myoferlin C2A (2DMH)

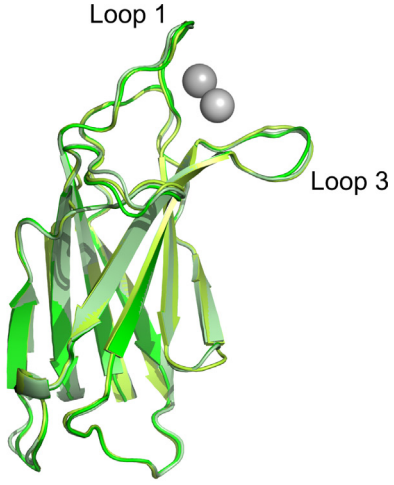

(b) Superposition of the three myoferlin C2A molecules in the crystallographic asymmetric unit

Fig. 3. Superimposed structures of myoferlin C2A with and without divalent cation. (a) Myoferlin C2A from the NMR-deposited structure (2DMH). (b) Superimposed molecules from the myoferlin C2A X-ray crystal structure (6EEL).

(site I, Fig. 2C) utilizes a reduced ligation shell with only three oxygen atoms contributed by the domain. The high-affinity site in dysferlin C2A, on the other hand, binds Ca^{2+} with one additional oxygen atom contributed by Asp-18 on loop 1 [34]. Therefore, relative to the same binding site in dysferlin C2A, the myoferlin C2A site I is incomplete (Fig. 2C). The more typical loop 1 aspartate (Asp-18 in dysferlin C2A) has been substituted with Gly-18 in myoferlin C2A. The majority of protein sequences identified as myoferlin in the Genbank database utilize a glycine at this locus (Fig. S2, 3). The ligation shell for the second binding site in myoferlin C2A (site II, Fig. 2C) is similar to that of dysferlin C2A [34].

Comparing NMR solution structures to a crystal structure can be problematic due to differences in buffer conditions and data collection temperatures; however, some key differences can be concluded. Superposition of the 20 NMR-derived ligand-free structures shows heterogeneity in conformation of loop 3, but less variation in loop 1 (Fig. 3a). In other C2 domains, loop 1 is flexible and therefore not modeled in X-ray structures, or it is completely absent from domain as in the case of otoferlin C2A [37]. Loop 1 in myoferlin C2A appears more rigid than other loop 1 sequences in C2 domains. Its rigidity can be traced to a difference in the primary sequence of a conserved stretch of residues that make up loop 1. In (type 1) synaptotagmin C2 domains, the …SDPYVK… motif, located at the C-terminal end of the loop 1 sequence, is essential for Ca^{2+} binding and is a hallmark of the C2 motif. Mutations of synaptotagmin C2 domains within this conserved motif eliminate Ca^{2+} binding *in vitro* [38,39], as well as Ca^{2+}-dependent exocytosis in *Drosophila in vivo* [40]. In myoferlin C2A, the corresponding sequence is …PDPIVS…, where the first serine in the conserved sequence has been replaced by a proline (Pro-20); Pro is conserved at this locus in the majority of myoferlin sequences (Figs. S2 and S3). In general proline augments the local structural rigidity of loops, and with two proline residues in close proximity within the same loop, we would therefore expect them to significantly decrease the conformational entropy of that loop. Indeed, in the NMR-derived, un-liganded domain, the average RMSD for backbone atoms for the residues in loop 1 (residues 10–22) is 0.52 Å, while the average RMSD between the 20 computed NMR structures is 0.78 Å for loop 3 (residues 71–79). The average RMSD value is 0.42 Å for all structures calculated using backbone atoms for the whole domain. Similarly, the relative rigidity of myoferlin C2A loop 1 is also reflected in the crystallographic *B*-factor of the liganded form of the domain. For loop 1 amino acids (residues 10–22), the average refined *B*-factor is 30.86 $Å^2$, while loop 3 (residues 71–79) is 44.26 $Å^2$. The refined *B*-factor for all atoms in myoferlin C2A domain, averaged from all three molecules in the asymmetric unit, is 26.94 $Å^2$ (Fig. 3b, Table 1).

Table 2. Summary of the ITC analysis of dysferlin C2A, dysferlin C2A M75A, myoferlin wild-type and myoferlin C2A F17A/I75A

Domain	n1	n2	ΔH_1 (kcal/mol)	ΔH_2 (kcal/mol)	ΔG_1 (kcal/mol)	ΔG_2 (kcal/mol)	$T\Delta S_1$ (kcal/mol)	$T\Delta S_2$ (kcal/mol)	K_{D1} (μM)	K_{D2} (μM)
Dys C2A WT	0.16 ± 0.06	2.68 ± 0.33	18.28 ± 2.28	−1.94 ± 0.29	−16.7 ± 14.42	−5.70 ± 1.22	34.98 ± 12.24	3.76 ± 1.18	0.70 ± 0.59	45.09 ± 4.30
Dys C2A M75A	0.30 ± 0.07	3.52 ± 0.17	47.78 ± 0.04	−1.80 ± 0.18	−9.65 ± 0.42	−5.53 ± 0.28	57.43 ± 0.42	3.73 ± 0.22	0.05 ± 0.03	64.14 ± 16.38
Myo C2A WT	2	–	−0.89 ± 0.05	–	−5.16 ± 1.02		4.27 ± 1.02	–	128.44 ± 49.44	–
Myo C2A F17A/I75A	1.79 ± 0.45	–	−0.47 ± 0.18	–	−4.71 ± −0.47	–	4.24 ± 0.43	–	312.23 ± 129.63	–

Dysferlin C2A was fit with a multiple site model, and myoferlin C2A was fit with an independent site model.

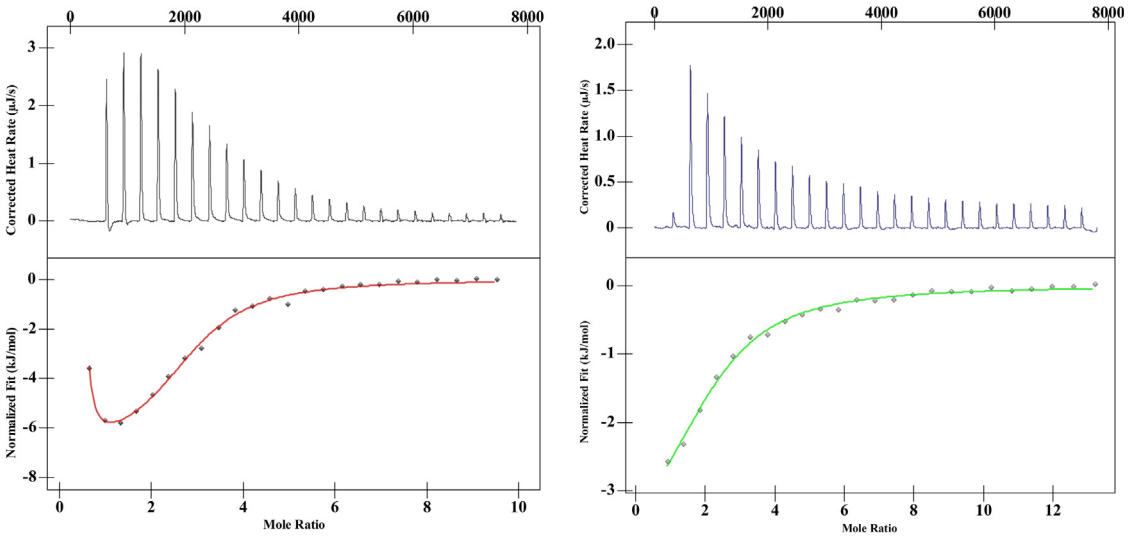

(a) Dysferlin C2A titrated with Ca^{2+}

(b) Myoferlin C2A titrated with Ca^{2+}

Fig. 4. Representative isothermal titration calorimetry (ITC) thermograms and their corresponding fitted curves of Ca^{2+} binding to wild-type (a) dysferlin C2A (red) and (b) myoferlin C2A (green). (a) Dysferlin C2A titrated with Ca^{2+}. (b) Myoferlin C2A titrated with Ca^{2+}.

Lipid-binding model for dysferlin and myoferlin C2A

As peripheral membrane binding domains, C2 domains often possess bulky hydrophobic residues at the tips of loops 1 and 3 to use as membrane anchors [36,41]. Myoferlin C2A possesses one bulky hydrophobic residue on loop 1 (Phe-17) and one hydrophobic residue on loop 3 (Ile-75), which is analogous to other C2 domains with membrane anchors. Dysferlin C2A has a single residue on loop 3 that could serve as a membrane anchor (Met-75); however, the membrane-binding potential of loop 1 is less clear. The sequence of Loop 1 of dysferlin C2A is His-Thr-Pro-Asp-Thr-Asp-Ile-Ser-Asp; therefore, it does possess a hydrophobic residue on loop 1 (Ile-19, Fig. 2D). If Ile-19 does indeed interact with membrane, it is positioned differently from other loop 1 binding residues. To ensure that the Ca^{2+}-binding pockets remained intact after mutagenesis, we measured the Ca^{2+}-binding properties of mutant dysferlin C2A and mutant myoferlin C2A. When we mutated Ile-19 on dysferlin C2A to an alanine residue (I19A), in addition to M75A, Ca^{2+} binding of the domain was abrogated (Fig. S5). It is likely that this residue may affect the overall shape of the calcium ion binding pocket; therefore, Ile-19 was excluded from further consideration. These results cannot, however, completely exclude Ile-19 as a membrane interacting residue without further experimentation. Our Ca^{2+}-binding measurements confirmed that the Ca^{2+}-binding pockets of the mutant C2 domains that we tested (dysferlin M75A and myoferlin F17A/I75A) remained functional and displayed similar binding values to that of the wild-type C2 domains (Table 2). To test the membrane-anchoring potential of the loop residues of myoferlin and dysferlin C2A, we used a co-sedimentation assay to compare wild-type and alanine mutations of the possible membrane-anchoring residues.

Dysferlin C2A did not significantly bind uncharged 100% phosphatidylcholine (PC) vesicles either with or without Ca^{2+} (Fig. 6). Upon exposure to a phospholipid surface with a large fraction of phosphoserine (60:40 PC/PS, phosphatidylcholine/phosphatidylserine), the Ca^{2+}-dependent component of binding appears. Thus, the Ca^{2+}-dependent enhancement, in the presence of Ca^{2+}, is ~5× greater relative to the Ca^{2+}-independent binding activity of the domain in 60:40 PC/PS (Fig. 6). The binding of the dysferlin C2A M75A mutation was reduced in 60:40 lipids with or without Ca^{2+}, suggesting that Met-75 is essential for membrane anchoring (Fig. 6). Myoferlin C2A, on the other hand, showed negligible binding throughout the range of phospholipids with or without Ca^{2+} (Fig. 6). Consistent with previously published data on the membrane binding specificity of myoferlin C2A [11], we did notice a minor component of Ca^{2+}-dependent phospholipid binding; however, in only very negatively charged phospholipid mixtures (50%:50% PC/PS). We did not observe significant binding of myoferlin C2A to membranes containing up to 5% phosphatidylinositol 4,5-bisphosphate (data not shown). The F17A/I75A mutation of myoferlin C2A displayed a minor Ca^{2+}-dependent effect relative to its Ca^{2+}-independent phospholipid binding component in the 50%:50% PC/PS lipid

mixture; however, the effect was weak in this assay (Fig. 6).

Kinetics of Ca^{2+}-dependent phospholipid binding by dysferlin C2A

To study the kinetics of Ca^{2+}-dependent phospholipid binding in dysferlin C2A, we used stopped-flow fluorescence spectrometry to determine the rate of binding of the C2 domains to a lipid surface in the presence of Ca^{2+} [42]. Similar to our co-sedimentation results, myoferlin C2A did not show appreciable binding to phospholipid by this method. Mixing of either Ca^{2+}/dysferlin C2A with liposomes, or lipids/dysferlin C2A with Ca^{2+}, resulted in changes in the fluorescence signals between the FRET acceptor incorporated into the vesicle and the donor Trp of dysferlin C2A (Fig. 7). Raw data traces from the stopped-flow spectrometer were fit with single exponentials to obtain kinetic values for either the lipid dependence or Ca^{2+} dependence of membrane binding by dysferlin C2A (Fig. 7A, C). Concerning the differences between experimental conditions, several features emerge from our kinetic measurements compared to similar experiments performed using synaptotagmin C2 domains. Ca^{2+}-dependent membrane binding by dysferlin C2A was markedly slower than that of the C2A domains of synaptotagmins 1 and 7, but was roughly comparable to that of the C2 domain from cytosolic phospholipase A2 [41,43]. Surprisingly, the observed rates (k_{obs}) for dysferlin C2A were almost invariant with respect to liposome concentration; however, k_{obs} exhibited a robust, linear dependence on [Ca^{2+}], suggesting a first-order dependence of lipid binding on [Ca^{2+}] in the concentration range measured. In this range of [Ca^{2+}] concentrations, the k_{on} for [Ca^{2+}] was 1.32×10^5 M^{-1} s^{-1}. This observation represents a striking contrast with other C2 domains, such as the C2A domain of synaptotagmin 1, which binds Ca^{2+} with very rapid, diffusion-limited kinetics, that is, 10^8 M^{-1} s^{-1} [44]. Lipid binding, not Ca^{2+} binding, is the rate-limiting step in the case of synaptotagmin 1 C2A. Therefore for dysferlin C2A, Ca^{2+}-binding appears to be kinetically limiting, a feature that distinguishes it from C2 domains of other proteins.

Discussion

Dysferlin (237 kDa) and myoferlin (230 kDa) participate in membrane fusion at different stages of muscle development and physiology. Dysferlin has been implicated in maintaining the integrity of cell membranes [45], while myoferlin is instrumental in the early stages of muscle development [46]. Overall, dysferlin and myoferlin are 68% similar (56% identical) at the primary sequence level. Indeed, the first C2A domains of both proteins are 57% similar (42% identical). Given the sequence identity shared between these two large proteins, one would naturally expect that they should function similarly or at least complement each other's function. However, based on our results, the C2A domains of myoferlin and dysferlin share relatively few biophysical properties. Here we show that the C2A domain of dysferlin has slow Ca^{2+}-dependent phospholipid-binding kinetics compared to other C2 domains. Furthermore, both myoferlin and dysferlin not only bind Ca^{2+} differently but also have distinct lipid-binding avidities that likely reflect their different roles in muscle physiology.

The overall tertiary structure of myoferlin C2A is similar to other type 2 (P-type) ferlin C2 domains. Both myoferlin and dysferlin C2A domains bind two calcium ions; however, each domain utilizes calcium ions for different purposes. Dysferlin C2A possesses one high-affinity site and one low-affinity site (Table 2, Fig. 4). The high-affinity Ca^{2+} site in dysferlin C2A is primarily structural, and its occupancy at this locus increases the likelihood of proper domain folding in C2A [34]. The lower-affinity site in dysferlin C2A responds to environmental Ca^{2+}, as it alters the surface electrostatics of the domain and prepares the domain for peripheral membrane attachment [34]. C2 domains coordinate calcium ions through a hexadentate arrangement of oxygen atoms contributed by both main-chain carbonyl oxygen atoms and side-chain oxygen atoms [47]. Most Ca^{2+}-binding C2 protein motifs have evolved to provide four equatorial and one axial oxygen atom. The sixth coordinating atom is typically contributed by phospholipids [48], hence providing a link between Ca^{2+} binding and phospholipid binding. Dysferlin C2A has this property; however, myoferlin is different. The affinity for Ca^{2+} of the myoferlin C2A domain is surprisingly low (K_D = 128 μM), and its low Ca^{2+}-binding affinity can be explained by two unique structural features. First, myoferlin C2A has substituted a glycine residue for the negatively charged residue that is typically located on loop 1. In fact, glycine at this locus on loop 1 is conserved in the vast majority of sequences labeled as myoferlin (Fig. S3). In the myoferlin C2A crystal structure, the hexadentate arrangement of oxygen atoms for the "I" calcium ion (Fig. 2C, D) is contributed by the side chains of Asp-21 and Asn-40, and the carbonyl oxygen from Lys-19. The remaining coordinating atoms in the crystal structure are provided by one water molecule, and/or two residues (Asp-94 and Gln-95) from symmetry-related molecules. The coordination of calcium ion "II" is similar to the lower-affinity calcium ion in dysferlin C2A.

The second adaptation of myoferlin can be explained by the rigidity of loop 1. The substitution of the first serine with a proline residue in the conserved … SDPYVK… motif likely contributes to the reduced calcium ion affinity. Since loop 1 in myoferlin C2A does not contribute side-chain oxygen atoms to Ca^{2+} binding, the change in the conformation of loop 1 cannot be linked to Ca^{2+} binding as with other C2

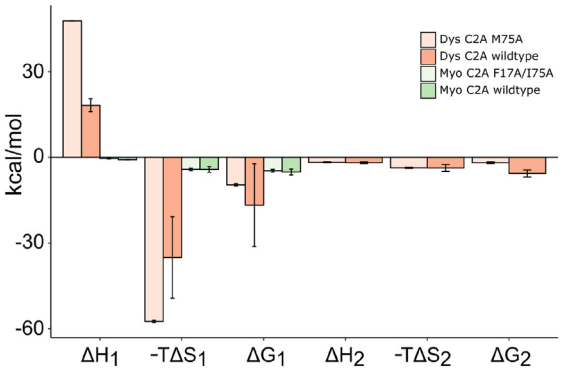

Fig. 5. Graphical summary from Table 2 of the thermodynamic parameters obtained from the ITC analysis of Ca^{2+} binding in myoferlin C2A and dysferlin C2A and the lipid-binding mutants.

domains. To bind calcium ion at all, the protein must therefore conserve the overall shape of the Ca^{2+} binding pocket via an alternative mechanism. Indeed, the entire loop 1 sequence is flanked by proline residues. The N-terminus of loop 1 begins with Pro-13, while the C-terminus ends with Pro-20, Asp-21, and Pro-22. Therefore, the conformation of loop 1 in myoferlin C2A is dominated by the restricted φ torsional angles accessible by its flanking proline residues. A similar conclusion has been made in the "RGD" loop of the HIVZ2 Tat protein [49]. The restricted conformational space of loop 1 is also reflected in the thermodynamic values obtained from cation binding (Table 2, Fig. 5). In the dysferlin C2A case, the relatively large enthalpic penalty for ions to bind at the high-affinity site is related to the folding dynamics of the domain as a function of Ca^{2+} occupancy (Table 2). The enthalpic barrier to binding is compensated by a net favorable ΔS term. The net favorable ΔS term includes the entropy changes due to the ordering of binding loops, in addition to the entropy changes due to the displacement of water molecules from the Ca^{2+}-binding site (Table 2, Fig. 5). Indeed, the ΔG of unfolding for dysferlin C2A is near 0 kcal/mol without $Ca^{(2+)}$ [34], so the domain samples a larger ensemble of unfolded states without Ca^{2+}. In myoferlin C2A, we measured a small enthalpic term complemented by a small, but favorable entropic term upon Ca^{2+} binding. Therefore, the thermodynamic values we measured for myoferlin C2A Ca^{2+} binding are consistent with the relatively small changes to the shape of the binding pocket, consistent with a more rigid binding pocket.

We predicted that myoferlin C2A should associate with phospholipid membranes in a similar manner to dysferlin and synaptotagmin C2A domains, as it has hydrophobic side chains located in homologous positions on loops 1 and 3. We also predicted that the C2 domains of myoferlin and dysferlin would prefer binding to negatively charged phospholipids similar to other C2 domains [50]. We measured avid dysferlin C2A association with a mixture of 60:40 PC/PS in a Ca^{2+}-dependent manner; myoferlin, on the other hand, did not show analogous degrees of binding to any of the phospholipid mixtures we tested with or without Ca^{2+} (Fig. 6). We did measure weak Ca^{2+}-dependent binding of myoferlin C2A with 50:50 PC/PS membranes [11] (Fig. 6), so a negatively charged phospholipid membrane is a component of myoferlin C2A phospholipid interaction. Therefore, even weak binding to anionic membranes likely reflects at least some electrostatic contribution to membrane docking for myoferlin C2A [41]. Indeed, a surface electrostatic representation of Ca^{2+}-bound myoferlin *versus* Ca^{2+}-bound dysferlin C2A shows a clear difference in the strength of the electrostatic surface potential relative to dysferlin C2A (Fig. 8a, b). The relatively weak surface electrostatics of myoferlin C2A is also reflected in the

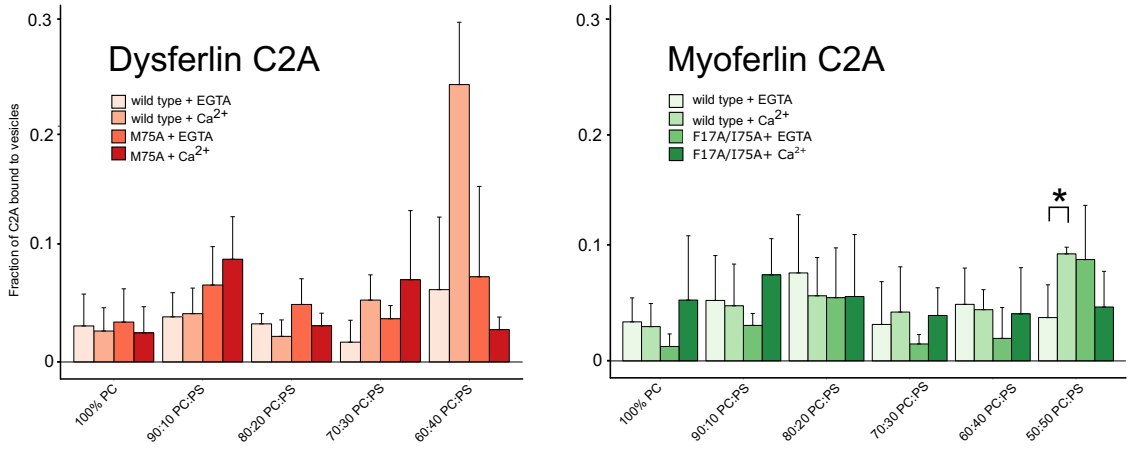

Fig. 6. Co-sedimentation assay results for dysferlin C2A and myoferlin C2A *versus* phospholipid. Error bars are standard deviation from at least four experiments. The "*" above the myoferlin C2A wild-type data denotes a significant statistical difference ($p<0.05$) between the two datas ets.

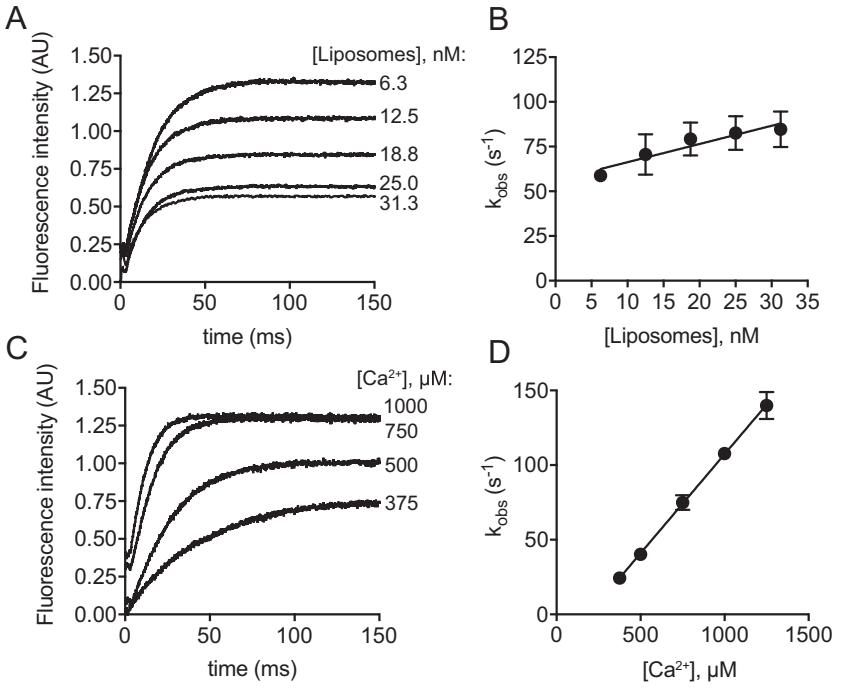

Fig. 7. (A) Representative dysferlin C2A stopped-flow traces; binding was monitored as a function of [liposome]. (B) Plot of k_{obs} from panel A. (C) Same as in panel A, except that binding was monitored as a function of [Ca^{2+}]. (D) Plot of k_{obs} from panel C. Error bars are the standard error from at least three independent experiments.

myoferlin C2A purification protocol as we could not use ion-exchange chromatography as with dysferlin C2A (Fig. 8b). In addition, we could not detect Ca^{2+}-dependent phospholipid binding of the myoferlin C2A double-mutant (Fig. 6); hence, these residues may contribute to a more tenuous protein–phospholipid association under our experimental conditions. Marty *et al.* [51] report a moderate Ca^{2+}-dependent,

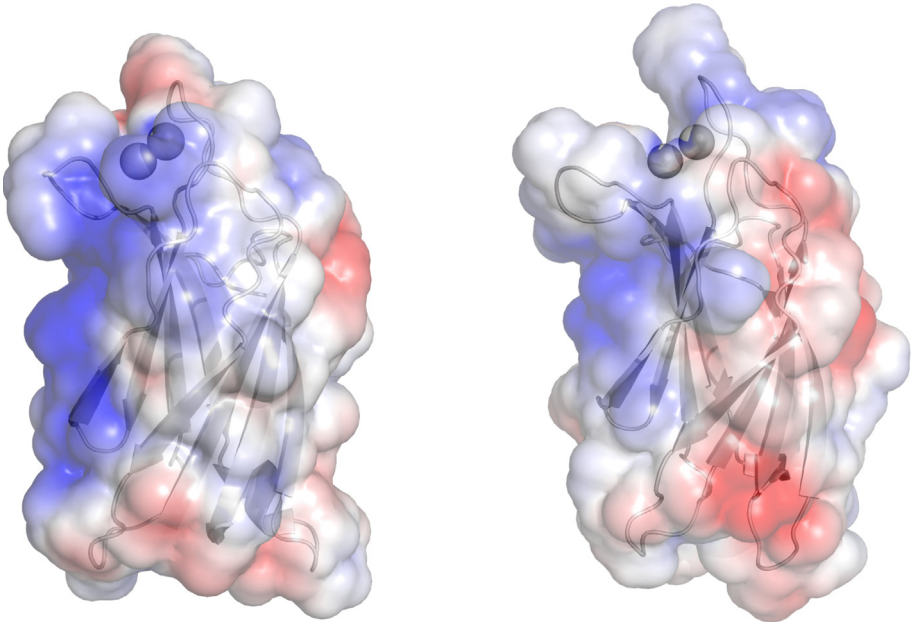

(a) Dysferlin C2A bound to Ca^{2+} (b) Myoferlin C2A bound to Ca^{2+}

Fig. 8. Electrostatic representation of (a) dysferlin C2A with Ca^{2+} and (b) myoferlin C2A with Ca^{2+}. Blue regions reflect positively charged zones on the surface of the domain. Red regions reflect negatively charged zones on the surface. Both molecules were contoured to ± 3 *k*T/e. (a) Dysferlin C2A bound to Ca^{2+}. (b) Myoferlin C2A bound to Ca^{2+}.

phospholipid-ordering effect of myoferlin C2A using a fluorescence polarization technique. It is possible that the exposed basic residues on the surface of myoferlin C2A loosely interact with negatively charged phospholipids to alter the order of lipids. Indeed, weak, tenuous protein–phospholipid interactions have been hypothesized in similar domains [52]. Another possibility to explain the anomalously weak interaction of myoferlin C2A with PS-containing membranes is that myoferlin C2A may be more selective for a specific membrane curvature or a different phospholipid packing arrangement relative to dysferlin C2A. For example, the C2 domains of synaptotagmin tend to bind to phospholipid mixtures that accentuate both electrostatics and highly curved surfaces [53].

Dysferlin and myoferlin are the most closely related members of ferlin protein family [54]. Despite their similarities, however, they are expressed in different stages of muscle cell growth and development and are associated with different diseases. The mechanism by which myoferlin interacts with Ca^{2+} and phospholipids has not been completely elucidated. In this study, we investigated the structural and functional characteristics of myoferlin C2A and compared it to the more extensively studied dysferlin C2A. We found significant differences between these seemingly similar domains that may partially explain the disparate physiological activity between dysferlin and myoferlin. We showed that myoferlin C2A binds calcium ions, but with 3-fold lower affinity than that of dysferlin C2A. We also showed that the phospholipid-binding activity of dysferlin C2A in the presence of Ca^{2+} is much higher than myoferlin C2A. We identified and established the significance of phospholipid-interacting residues of the dysferlin (Met-75). Our M75A mutant of dysferlin C2A reduced Ca^{2+}-dependent phospholipid-binding activity of dysferlin C2A, while the Ca^{2+}-binding activity was preserved. The association of myoferlin C2A to PC/PS (50:50) liposomes in the presence of Ca^{2+} was also reduced in the F17A and I75A mutants, albeit weakly. Furthermore, we studied the kinetics of dysferlin C2A interaction with phospholipids. Our stopped-flow spectrometry results indicate that the kinetics of the dysferlin C2A Ca^{2+}-dependent phospholipid interaction are mainly a function of Ca^{2+} concentration. In dysferlin C2A, while increasing lipid concentration provoked only small increases in k_{obs}, we observed a steep linear dependence of kobs on [Ca^{2+}]. To the best of our understanding, this indicates that formation of the C2A – Ca^{2+} complex, that is, Ca^{2+}-binding, is rate limiting rather than binding of the complex to lipids. Dysferlin C2A represents the first example of a C2 domain for which membrane association is dependent on the concentration of the C2A – Ca^{2+} complex, although the lipid *versus* Ca^{2+} dependence of membrane association kinetics has not been formally established for most C2 domains. Presumably, elevated cytoplasmic calcium ion concentration is among the stimulatory signals for dysferlin's action, so the protein should be capable of differentiating between the elevation of transient myocyte cytoplasmic calcium ion concentration and those transients associated with sarcolemmal damage. A "slow" Ca^{2+} sensor that is only activated by prolonged Ca^{2+} transients could serve this function. The Ca^{2+}-sensitive kinetics that we observed for C2A may allow dysferlin to act as a Ca^{2+} sensor for sarcolemmal damage in an environment where large Ca^{2+} transients are commonplace. Finally, our crystal structure of divalent-bound myoferlin C2A together with our thermodynamics analysis suggests that unlike dysferlin C2A, loop 1 in myoferlin C2A is less flexible, and there is likely a conformational change in its loop 3 upon Ca^{2+} binding. Future studies will include the analysis of the other domains of ferlin family members to understand their role in the total activity of these proteins, and why mutations lead to disease.

Methods and Materials

Cloning, expression, and purification of C2A domains

The cloning of dysferlin C2A was described previously [34]. The myoferlin C2A gene (1–125) was assembled by Genewiz based on the human myoferlin sequence from GENBANK:AAF27176.1. The C-terminus of myoferlin C2A was determined based on the alignment of myoferlin with the dysferlin C2A crystal structure (4IHB). The primary sequence for myoferlin C2A was reverse-translated and optimized for *Escherichia coli* expression. The resulting nucleotide sequence was cloned into the pET-based p202 expression vector for subsequent expression. Dysferlin and myoferlin C2A wild-type and mutant domain expression plasmids were transformed into BL21 (DE3)-competent cells and spread onto Luria Broth agar plates containing 50 μg/mL kanamycin and incubated at 37 ° C overnight. Isolated colonies were picked and used to start a 50 mL Luria Broth containing 50 μg/mL kanamycin, and the culture was incubated overnight at 37 ° C while shaking at 250 rpm. 10 mL of this culture was used to inoculate a 1 L Terrific Broth culture also containing 50 μg/mL kanamycin at 37 ° C and 250 rpm. At OD_{600} = 2.0, the culture was cooled to 18 ° C and the protein expression was induced with the addition of 400 μL of 1 M isopropyl β-D-1-thiogalactopyranoside (IPTG). After 12 h of incubation, cells were harvested using a Beckman JLA-8.1000 rotor at 5000 rpm (6227*g*) and flash frozen in liquid nitrogen until ready for use. Next, cells were thawed in lysis buffer [20 mM HEPES (pH 7.4), 150 mM NaCl, 5 mM $CaCl_2$], ruptured using a Microfluidizer, and spun using a Beckman JA-20 rotor at 19,500 rpm (45,900*g*) for 45 min. The supernatant was passed through a Ni-NTA affinity column which was equilibrated with lysis buffer. The column then was washed with 150 mL lysis buffer,

followed by a wash in lysis buffer plus 30 mM imidazole. Finally, His_6-MBP-C2A was eluted with 80 mL lysis buffer including 300 mM imidazole. The resulting fusion protein was cleaved with tobacco etch virus protease (TEV) overnight at 4 ° C. At this step, all proteins were buffer-exchanged into 20 mM Hepes (pH 7.4), 50 mM NaCl, and 5 mM $CaCl_2$ for further purification using ion-exchange chromatography. In the case of dysferlin, SP-Sepharose column was used to separate C2A from MBP, TEV protease, and uncleaved fusion proteins. A 0- to 1-M NaCl gradient was applied to the column, and dysferlin C2A wild-type and mutant domains were eluted in fractions starting at a conductivity of 38 mS/cm. In the case of myoferlin, protein solutions were loaded onto QAE-Sepharose column and myoferlin C2A wild-type or mutant myoferlin C2A domains came off in the flow-through. We tried SP-Sepharose column for myoferlin, and still myoferlin C2A domain mostly came off in the flow-through. In either case, the solution containing the protein of interest was concentrated and loaded onto a Superdex 75 column to remove the remaining contaminations. Purity was assessed using SDS PAGE Stain-Free gels from BioRad (Fig. S1), and protein concentrations were quantitated by OD_{280} using each proteins calculated extinction coefficient.

Crystallization and data collection

Purified myoferlin C2A domain (10 mg/mL) was crystallized in 0.1 M Bis–Tris (pH 6.5), 20% PEG 3350, and 0.3 M $SrCl_2$. Crystals were grown at 23 ° C. The crystals were captured into nylon loops and frozen in liquid N_2. Initial data sets were collected on a Rigaku ScreenMachine. Subsequent data sets were collected at SSRL beamline 7-1. The wavelength of the final data sets was 0.9796 Å, and the data were collected at 90 K. X-ray data were processed with imosflm [55], and the data were scaled using AIMLESS as a part of the CCP4 package [56]. The X-ray crystal structure was solved using molecular replacement techniques (Phaser) [57] and subsequently refined using Phenix [58].

Isothermal titration calorimetry

The ITC buffer, containing 150 mM KCl, and 20 mM HEPES pH 7.4, was passed through a Bio-Rad Chelex 100 resin to remove cation impurities and filtered using 0.22-μm membrane filter. The Ca^{2+} stock solution was prepared by diluting sterile and filtered 2.0 M $CaCl_2$ stock solution purchased from Research Products International with the ITC buffer. In addition, the proteins were buffer exchanged into the ITC buffer using PD-10 columns from GE Healthcare. Each experiment was repeated at least three times with 200 rpm mixing at 15 ° C. The best results obtained using a protein concentration ranging from 150 to 400 μM and a titrant (Ca^{2+}) concentration of either 5 or 10 mM. All experimental repeats corresponding to each protein sample were performed using a constant $CaCl_2$ concentration. The analysis was performed using NanoAnalyze software. We fit the raw data using a multiple binding sites model for dysferlin C2A and an independent model for myoferlin C2A (with n = 2).

Liposome preparation

1-palmitoyl-2-oleoyl-glycero-3-phosphocholine (POPC), 1-palmitoyl-2-oleoyl-sn-glycero-3-phospho-L-serine (POPS), and 1,2-dioleoyl-sn-glycero-3-phosphoethanolamine-*N*-(5-dimethylamino-1-naphthalenesulfonyl) (dansyl-PE) were purchased from Avanti Polar Lipids. Phospholipids in chloroform were mixed to obtain the desired molar ratio, and residual chloroform was then evaporated using nitrogen gas. Dried phospholipids were put under vacuum overnight to remove the chloroform residues. The phospholipids were then resuspended in a buffer (200 mM NaCl and 20 mM HEPES, pH 7.4) that was passed through Bio-Rad Chelex 100 resin to remove divalent cations. The phospholipids were allowed to rehydrate over 15 min while vortexed and then were sonicated liposomes (100 nm) were prepared by extrusion through 100-nm polycarbonate filters using an Avanti Mini Extruder. The size of vesicles was confirmed to be 100 ± 12 nm, as determined using a Malvern Zetasizer Nano ZS (data not shown). Liposome concentration was calculated assuming a population of unilamellar liposomes of 5-nm thickness and 100-nm outer diameter at 0.71 nm^2 per lipid headgroup. This resulted in an estimate of 8.0 $\times 10^4$ lipid molecules per liposome, for example, 10 nm [liposomes] = 0.8 mM [lipid].

Stopped-flow rapid mixing experiments

Kinetics experiments were carried out using an Applied Photophysics SX.18MV stopped-flow spectrometer as described [44]. Large (~100 nm) unilamellar liposomes containing 65% Popc, 30% Pops, and 5% dansyl-PE were prepared, and FRET experiments were carried out by excitation of tryptophan at 285 nm and measuring the emission of dansyl-PE using a 523-nm band-pass filter. All experimental data represent three independent experiments.

Sedimentation assay

As described previously [25,59]. In a 100-μL total reaction volume, liposomes with various POPC/POPS ratio were mixed with protein and either EGTA or Ca^{2+}. The proteins were also buffer exchanged into the Chelex-treated buffer used in preparation of liposomes to remove any Ca^{2+} contamination. The final concentration of each component was as follows: 1 mM liposomes, 4 μM protein, and either 0.2 mM EGTA or 1 mM $CaCl_2$. The samples were allowed to incubate for 15 min in 37 ° C and then centrifuged at 65,000 rpm

(183,000*g*) using a Beckman TLA-100 rotor for 45 min in a Beckman Optima MAX-E table-top ultracentrifuge. In most cases, analysis of the supernatant is preferable to analysis of the pellet because it requires reduced sample handling, produces more robust results, and is amenable to large scale comparisons with other C2 domains [53]. Therefore, equal amounts of the supernatants were loaded to SDS-PAGE and were imaged and quantified using a Bio-Rad Criterion Stain Free Imaging System Gel Imager and Image Lab software (Fig S4). This technology does not require staining and destaining steps, providing a highly sensitive and reliable method in protein quantification that is equal or better than Coomassie staining. Each experiment was repeated at least three times, and the errors are presented as standard deviation. Student's *t*-test statistical analysis was performed to test the significance of the difference observed between the measurements.

Equilibrium co-sedimentation control experiment

The co-sedimentation assay has been a common biochemical technique to study protein–phospholipid interactions, especially in ferlins and synaptotagmins. In co-sedimentation experiments, additional controls need to be considered to assure that the observed interaction is a direct result of protein-vesicle interaction. We considered three control experiments for each protein: the input (protein only), protein + EGTA control, and protein + Ca^{2+} control (Fig. S4). These controls lack lipid vesicles and reveal aggregation due to possible interaction of proteins with either EGTA or Ca^{2+}. We observed no detectable depletion in the amount of protein in the supernatant in our control experiments, which strongly suggests that C2A proteins do not aggregate or pellet when combined with Ca^{2+} or EGTA.

RMSD calculations

All RMSD values were computed using the method as implemented in PyMOL [60].

Accession numbers

Coordinates and structure factors have been deposited in the Protein Data Bank with accession number 6EEL.

Acknowledgments

Research reported in this publication was supported in part by the Jain Foundation and The National Institute of Arthritis and Musculoskeletal and Skin Diseases of the National Institutes of Health under Award Number R01AR063634. Use of the Stanford Synchrotron Radiation Lightsource, SLAC National Accelerator Laboratory, is supported by the U.S. Department of Energy, Office of Science, Office of Basic Energy Sciences under Contract No. DE-AC02-76SF00515. The SSRL Structural Molecular Biology Program is supported by the DOE Office of Biological and Environmental Research, and by the National Institutes of Health, National Institute of General Medical Sciences (including P41GM103393). The contents of this publication are solely the responsibility of the authors and do not necessarily represent the official views of NIGMS or NIH. We also would like to thank Dr. Michael Latham, Dr. Mariana Fiori, Matthew Dominguez, Jacob Gendelman, and Jon McCord for their help in reviewing this publication.

Appendix A. Supplementary data

Supplementary data to this article can be found online at https://doi.org/10.1016/j.jmb.2019.04.006.

Received 1 January 2019;
Received in revised form 4 April 2019;
Accepted 4 April 2019
Available online 18 April 2019

Keywords:
ferlin proteins;
C2 domains;
X-ray crystallography

Abbreviations used:
PC, phosphotidylcholine; PS, phosphoserine; ITC, isothermal titration calorimetry; Popc, 1-palmitoyl-2-oleoyl-glycero-3-phosphocholine; Pops, 1-palmitoyl-2-oleoyl-sn-glycero-3-phospho-L-serine; Dansyl-PE, 1,2-dioleoyl-sn-glycero-3-phosphoethanolamine-*N*-(5-dimethylamino-1-naphthalenesulfonyl).

References

[1] R. Han, Muscle membrane repair and inflammatory attack in dysferlinopathy, Skelet. Muscle 1 (1) (2011) 10, https://doi.org/10.1186/2044-5040-1-10 (URL https://doi.org/10.1186/2044-5040-1-10).

[2] R. Han, E.M. Frett, J.R. Levy, E.P. Rader, J.D. Lueck, D. Bansal, S.A. Moore, R. Ng, D.B.-V. de Bernabé, J.A. Faulkner, K.P. Campbell, Genetic ablation of complement C3 attenuates muscle pathology in dysferlin-deficient mice, J. Clin. Investig. 120 (12) (2010) 4366–4374, https://doi.org/10.1172/jci42390 (URL https://doi.org/10.1172/jci42390).

[3] R. Rawat, T.V. Cohen, B. Ampong, D. Francia, A. Henriques-Pons, E.P. Hoffman, K. Nagaraju, Inflammasome up-regulation and activation in dysferlin-deficient skeletal muscle, Am. J. Pathol. 176 (6) (2010) 2891–2900, https://doi.org/

10.2353/ajpath.2010.090058 (URL https://doi.org/10.2353/ajpath.2010.090058).
[4] T. Weiler, R. Bashir, L.V. Anderson, K. Davison, J.A. Moss, S. Britton, E. Nylen, S. Keers, E. Vafiadaki, C.R. Greenberg, C.R. Bushby, K. Wrogemann, Identical mutation in patients with limb girdle muscular dystrophy type 2B or Miyoshi myopathy suggests a role for modifier gene(s), Hum. Mol. Genet. 8 (5) (1999) 871–877.
[5] N.R. Davenport, K.J. Sonnemann, K.W. Eliceiri, W.M. Bement, Membrane dynamics during cellular wound repair, Mol. Biol. Cell 27 (14) (2016) 2272–2285, https://doi.org/10.1091/mbc.e16-04-0223 (URL https://doi.org/10.1091/mbc.e16-04-0223).
[6] N.R. Davenport, W.M. Bement, Cell repair: revisiting the patch hypothesis, Commun. Integr. Biol. 9 (6) (2016), e1253643. https://doi.org/10.1080/19420889.2016.1253643 (URL https://doi.org/10.1080/19420889.2016.1253643).
[7] D. Bansal, K. Miyake, S.S. Vogel, S. Groh, C.C. Chen, R. Williamson, P.L. McNeil, K.P. Campbell, P.L. McNeil, Defective membrane repair in dysferlin-deficient muscular dystrophy, Nature 423 (6936) (2003) 168–172.
[8] A. Lek, F.J. Evesson, R.B. Sutton, K.N. North, S.T. Cooper, Ferlins: regulators of vesicle fusion for auditory neurotransmission, receptor trafficking and membrane repair, Traffic 13 (2) (2011) 185–194, https://doi.org/10.1111/j.1600-0854.2011.01267.x (URL https://doi.org/10.1111/j.1600-0854.2011.01267.x).
[9] D.B. Davis, A.J. Delmonte, C.T. Ly, E.M. McNally, Myoferlin, a candidate gene and potential modifier of muscular dystrophy, Hum. Mol. Genet. 9 (2) (2000) 217–226.
[10] A.R. Demonbreun, A.D. Posey, K. Heretis, K.A. Swaggart, J.U. Earley, P. Pytel, E.M. McNally, Myoferlin is required for insulin-like growth factor response and muscle growth, FASEB J. 24 (4) (2010) 1284–1295, https://doi.org/10.1096/fj.09-136309 (URL https://doi.org/10.1096/fj.09-136309).
[11] D.B. Davis, K.R. Doherty, A.J. Delmonte, E.M. McNally, Calcium-sensitive phospholipid binding properties of normal and mutant ferlin C2 domains, J. Biol. Chem. 277 (25) (2002) 22883–22888, https://doi.org/10.1074/jbc.m201858200 (URL https://doi.org/10.1074/jbc.m201858200).
[12] K.R. Doherty, A.R. Demonbreun, G.Q. Wallace, A. Cave, A.D. Posey, K. Heretis, P. Pytel, E.M. McNally, The endocytic recycling protein EHD2 interacts with myoferlin to regulate myoblast fusion, J. Biol. Chem. 283 (29) (2008) 20252–20260, https://doi.org/10.1074/jbc.m802306200 (URL https://doi.org/10.1074/jbc.m802306200).
[13] P.N. Bernatchez, L. Acevedo, C. Fernandez-Hernando, T. Murata, C. Chalouni, J. Kim, H. Erdjument-Bromage, V. Shah, J.-P. Gratton, E.M. McNally, P. Tempst, W.C. Sessa, Myoferlin regulates vascular endothelial growth factor receptor-2 stability and function, J. Biol. Chem. 282 (42) (2007) 30745–30753, https://doi.org/10.1074/jbc.m704798200 (URL https://doi.org/10.1074/jbc.m704798200).
[14] C. Leung, C. Yu, M.I. Lin, C. Tognon, P. Bernatchez, Expression of myoferlin in human and murine carcinoma tumors, Am. J. Pathol. 182 (5) (2013) 1900–1909, https://doi.org/10.1016/j.ajpath.2013.01.041 (URL https://doi.org/10.1016/j.ajpath.2013.01.041).
[15] A. Turtoi, A. Blomme, A. Bellahcene, C. Gilles, V. Hennequiere, P. Peixoto, E. Bianchi, A. Noel, E.D. Pauw, E. Lifrange, P. Delvenne, V. Castronovo, Myoferlin is a key regulator of EGFR activity in breast cancer, Cancer Res. 73 (17) (2013) 5438–5448, https://doi.org/10.1158/0008-5472.can-13-1142 (URL https://doi.org/10.1158/0008-5472.can-13-1142).
[16] D. Song, G. Ko, J. Lee, J. Lee, G.-W. Lee, H. Kim, J. Yang, R. Heo, G. Roh, S.-Y. Han, D. Kim, Myoferlin expression in non-small cell lung cancer: prognostic role and correlation with VEGFR-2 expression, Oncol. Lett. 11 (2) (2015) 998–1006, https://doi.org/10.3892/ol.2015.3988 (URL https://doi.org/10.3892/ol.2015.3988).
[17] D. Song, G. Ko, J. Lee, J. Lee, J. Yang, M. Kim, H. An, M. Kang, K. Jeon, D. Kim, Prognostic role of myoferlin expression in patients with clear cell renal cell carcinoma, Oncotarget 8 (51) (2017), https://doi.org/10.18632/oncotarget.21645 (URL https://doi.org/10.18632/oncotarget.21645).
[18] C. Hermanns, V. Hampl, K. Holzer, A. Aigner, J. Penkava, N. Frank, D.E. Martin, K.C. Maier, N. Waldburger, S. Roessler, M. Goppelt-Struebe, I. Akrap, A. Thavamani, S. Singer, A. Nordheim, T. Gudermann, S. Muehlich, The novel MKL target gene myoferlin modulates expansion and senescence of hepatocellular carcinoma, Oncogene 36 (24) (2017) 3464–3476, https://doi.org/10.1038/onc.2016.496 (URL https://doi.org/10.1038/onc.2016.496).
[19] R. Li, W.E. Ackerman, C. Mihai, L.I. Volakis, S. Ghadiali, D.A. Kniss, Myoferlin depletion in breast cancer cells promotes mesenchymal to epithelial shape change and stalls invasion, PLoS ONE 7 (6) (2012), e39766. https://doi.org/10.1371/journal.pone.0039766 (URL https://doi.org/10.1371/journal.pone.0039766).
[20] L.I. Volakis, R. Li, W.E. Ackerman, C. Mihai, M. Bechel, T.L. Summerfield, C.S. Ahn, H.M. Powell, R. Zielinski, T.J. Rosol, S.N. Ghadiali, D.A. Kniss, Loss of myoferlin redirects breast cancer cell motility towards collective migration, PLoS ONE 9 (2) (2014), e86110. https://doi.org/10.1371/journal.pone.0086110 (URL https://doi.org/10.1371/journal.pone.0086110).
[21] K. Fahmy, A. Gonzalez, M. Arafa, P. Peixoto, A. Bellahcène, A. Turtoi, P. Delvenne, M. Thiry, V. Castronovo, O. Peulen, Myoferlin plays a key role in VEGFA secretion and impacts tumor-associated angiogenesis in human pancreas cancer, Int. J. Cancer 138 (3) (2015) 652–663, https://doi.org/10.1002/ijc.29820 (URL https://doi.org/10.1002/ijc.29820).
[22] A. Blomme, B. Costanza, P. de Tullio, M. Thiry, G.V. Simaeys, S. Boutry, G. Doumont, E.D. Valentin, T. Hirano, T. Yokobori, S. Gofflot, O. Peulen, A. Bellahcène, F. Sherer, C.L. Goff, E. Cavalier, A. Mouithys-Mickalad, F. Jouret, P.G. Cusumano, E. Lifrange, R.N. Muller, S. Goldman, P. Delvenne, E.D. Pauw, M. Nishiyama, V. Castronovo, A. Turtoi, Myoferlin regulates cellular lipid metabolism and promotes metastases in triple-negative breast cancer, Oncogene 36 (15) (2016) 2116–2130, https://doi.org/10.1038/onc.2016.369 (URL https://doi.org/10.1038/onc.2016.369).
[23] A. Blomme, K. Fahmy, O. Peulen, B. Costanza, M. Fontaine, I. Struman, D. Baiwir, E. de Pauw, M. Thiry, A. Bellahcène, V. Castronovo, A. Turtoi, Myoferlin is a novel exosomal protein and functional regulator of cancer-derived exosomes, Oncotarget 7 (50) (2016), https://doi.org/10.18632/oncotarget.13276 (URL https://doi.org/10.18632/oncotarget.13276).
[24] J. Pei, B.-H. Kim, N.V. Grishin, PROMALS3d: a tool for multiple protein sequence and structure alignments, Nucleic Acids Res. 36 (7) (2008) 2295–2300, https://doi.org/10.1093/nar/gkn072 (URL https://doi.org/10.1093/nar/gkn072).
[25] F.M. Harsini, S. Chebrolu, K.L. Fuson, M.A. White, A.M. Rice, R.B. Sutton, FerA is a membrane-associating four-helix bundle domain in the ferlin family of membrane-fusion proteins, Sci. Rep. 8 (1) (2018), https://doi.org/10.1038/

s41598-018-29184-1 (URL https://doi.org/10.1038/s41598-018-29184-1).
[26] A. Sula, A.R. Cole, C. Yeats, C. Orengo, N.H. Keep, Crystal structures of the human dysferlin inner DysF domain, BMC Struct. Biol. 14 (1) (2014) 3, https://doi.org/10.1186/1472-6807-14-3 (URL https://doi.org/10.1186/1472-6807-14-3).
[27] X. Shao, C. Li, I. Fernandez, X. Zhang, T.C. Sudhof, J. Rizo, Synaptotagmin–syntaxin interaction: the C2 domain as a Ca^{2+}-dependent electrostatic switch, Neuron 18 (1) (1997) 133–142.
[28] C. Therrien, S.D. Fulvio, S. Pickles, M. Sinnreich, Characterization of lipid binding specificities of dysferlin C2 domains reveals novel interactions with phosphoinositides, Biochemistry 48 (11) (2009) 2377–2384, https://doi.org/10.1021/bi802242r (URL https://doi.org/10.1021/bi802242r).
[29] N. Abdullah, M. Padmanarayana, N.J. Marty, C.P. Johnson, Quantitation of the Ca^{2+} and membrane binding properties of the C2 domains of dysferlin, Biophys. J. 106 (2) (2014) 382–389, https://doi.org/10.1016/j.bpj.2013.11.4492 (URL https://doi.org/10.1016/j.bpj.2013.11.4492).
[30] A. Lek, F.J. Evesson, F.A. Lemckert, G.M. Redpath, A.K. Lueders, L. Turnbull, C.B. Whitchurch, K.N. North, S.T. Cooper, Calpains, cleaved mini-dysferlinC72, and L-type channels underpin calcium-dependent muscle membrane repair, J. Neurosci. 33 (12) (2013) 5085–5094.
[31] G.M. Redpath, N. Woolger, A.K. Piper, F.A. Lemckert, A. Lek, P.A. Greer, K.N. North, S.T. Cooper, Calpain cleavage within dysferlin exon 40a releases a synaptotagmin-like module for membrane repair, Mol. Biol. Cell 25 (19) (2014) 3037–3048.
[32] W. Lostal, M. Bartoli, C. Roudaut, N. Bourg, M. Krahn, M. Pryadkina, P. Borel, L. Suel, J.A. Roche, D. Stockholm, R.J. Bloch, N. Levy, R. Bashir, I. Richard, Lack of correlation between outcomes of membrane repair assay and correction of dystrophic changes in experimental therapeutic strategy in dysferlinopathy, PLoS ONE 7 (5) (2012), e38036. https://doi.org/10.1371/journal.pone.0038036 (URL https://doi.org/10.1371/journal.pone.0038036).
[33] Y. Cheng, S.M. Sequeira, L. Malinina, V. Tereshko, T.H. Sollner, D.J. Patel, Crystallographic identification of Ca2+ and Sr2+ coordination sites in synaptotagmin I C2B domain, Protein Sci. 13 (10) (2004) 2665–2672.
[34] K. Fuson, A. Rice, R. Mahling, A. Snow, K. Nayak, P. Shanbhogue, A.G. Meyer, G.M. Redpath, A. Hinderliter, S.T. Cooper, R.B. Sutton, Alternate splicing of dysferlin C2A confers Ca^{2+}-dependent and Ca^{2+}-independent binding for membrane repair, Structure 22 (1) (2014) 104–115.
[35] T. Nagashima, F. Hayashi, S. Yokoyama, Solution Structure of the first C2 Domain of Human Myoferlin, Oct 2006https://doi.org/10.2210/pdb2dmh/pdb (URL https://doi.org/10.2210/pdb2dmh/pdb).
[36] E.R. Chapman, A.F. Davis, Direct interaction of a Ca^{2+}-binding loop of synaptotagmin with lipid bilayers, J. Biol. Chem. 273 (22) (1998) 13995–14001, https://doi.org/10.1074/jbc.273.22.13995 (URL https://doi.org/10.1074/jbc.273.22.13995).
[37] S. Helfmann, P. Neumann, K. Tittmann, T. Moser, R. Ficner, E. Reisinger, The crystal structure of the C2A domain of otoferlin reveals an unconventional top loop region, J. Mol. Biol. 406 (3) (2011) 479–490, https://doi.org/10.1016/j.jmb.2010.12.031 (URL https://doi.org/10.1016/j.jmb.2010.12.031).
[38] M.C. Shields, M.R. Bowers, M.M. Fulcer, M.K. Bollig, P.J. Rock, R.B. Sutton, A.D. Vrailas-Mortimer, H. Lochmüller, R.G. Whittaker, R. Horvath, N.E. Reist, *Drosophila* studies support a role for a presynaptic synaptotagmin mutation in a human congenital myasthenic syndrome, PLoS ONE 12 (9) (2017), e0184817. https://doi.org/10.1371/journal.pone.0184817 (URL https://doi.org/10.1371/journal.pone.0184817).
[39] J. Ubach, X. Zhang, X. Shao, T.C. Südhof, J. Rizo, Ca^{2+} binding to synaptotagmin: how many calcium ions bind to the tip of a C2-domain? EMBO J. 17 (14) (1998) 3921–3930, https://doi.org/10.1093/emboj/17.14.3921 (URL https://doi.org/10.1093/emboj/17.14.3921).
[40] A. DiAntonio, T.L. Schwarz, The effect on synaptic physiology of synaptotagmin mutations in *Drosophila*, Neuron 12 (4) (1994) 909–920.
[41] D.S. Brandt, M.D. Coffman, J.J. Falke, J.D. Knight, Hydrophobic contributions to the membrane docking of synaptotagmin 7 C2A domain: mechanistic contrast between isoforms 1 and 7, Biochemistry 51 (39) (2012) 7654–7664, https://doi.org/10.1021/bi3007115 (URL https://doi.org/10.1021/bi3007115).
[42] E. Hui, J. Bai, E.R. Chapman, Ca^{2+}-triggered simultaneous membrane penetration of the tandem C2-domains of synaptotagmin I, Biophys. J. 91 (5) (2006) 1767–1777.
[43] E.A. Nalefski, M.A. Wisner, J.Z. Chen, S.R. Sprang, M. Fukuda, K. Mikoshiba, J.J. Falke, C2 domains from different Ca^{2+} signaling pathways display functional and mechanistic diversity, Biochemistry 40 (10) (2001) 3089–3100.
[44] A.F. Davis, J. Bai, D. Fasshauer, M.J. Wolowick, J.L. Lewis, E.R. Chapman, Kinetics of synaptotagmin responses to Ca^{2+} and assembly with the core SNARE complex onto membranes, Neuron 24 (2) (1999) 363–376, https://doi.org/10.1016/s0896-6273(00)80850-8 URL https://doi.org/10.1016/s0896-6273(00)80850-8).
[45] D. Bansal, K.P. Campbell, Dysferlin and the plasma membrane repair in muscular dystrophy, Trends Cell Biol. 14 (4) (2004) 206–213.
[46] K.R. Doherty, A. Cave, D.B. Davis, A.J. Delmonte, A. Posey, J.U. Earley, M. Hadhazy, E.M. McNally, Normal myoblast fusion requires myoferlin, Development 132 (24) (2005) 5565–5575.
[47] J.J. Falke, S.K. Drake, A.L. Hazard, O.B. Peersen, Molecular tuning of ion binding to calcium signaling proteins, Q. Rev. Biophys. 27 (3) (1994) 219–290.
[48] N. Verdaguer, S. Corbalan-Garcia, W.F. Ochoa, I. Fita, J.C. Gómez-Fernández, Ca^{2+} bridges the C2 membrane-binding domain of protein kinase Cα directly to phosphatidylserine, EMBO J. 18 (22) (1999) 6329–6338, https://doi.org/10.1093/emboj/18.22.6329 (URL https://doi.org/10.1093/emboj/18.22.6329).
[49] J. Liu, H. Tan, B. Rost, Loopy proteins appear conserved in evolution, J. Mol. Biol. 322 (1) (2002) 53–64, https://doi.org/10.1016/s0022-2836(02)00736-2 (URL https://doi.org/10.1016/s0022-2836(02)00736-2).
[50] X. Zhang, J. Rizo, T.C. Südhof, Mechanism of phospholipid binding by the C2A-domain of synaptotagmin 1, Biochemistry 37 (36) (1998) 12395–12403, https://doi.org/10.1021/bi9807512 (URL https://doi.org/10.1021/bi9807512).
[51] N.J. Marty, C.L. Holman, N. Abdullah, C.P. Johnson, The C2 domains of otoferlin, dysferlin, and myoferlin alter the packing of lipid bilayers, Biochemistry 52 (33) (2013) 5585–5592, https://doi.org/10.1021/bi400432f (URL https://doi.org/10.1021/bi400432f).
[52] H.M. Khan, T. He, E. Fuglebakk, C. Grauffel, B. Yang, M.F. Roberts, A. Gershenson, N. Reuter, A role for weak electrostatic interactions in peripheral membrane protein binding, Biophys. J. 110 (6) (2016) 1367–1378, https://doi.org/10.1016/j.bpj.2016.02.020 (URL https://doi.org/10.1016/j.bpj.2016.02.020).
[53] E. Hui, C.P. Johnson, J. Yao, F.M. Dunning, E.R. Chapman, Synaptotagmin-mediated bending of the target membrane is a critical step in Ca^{2+}-regulated fusion, Cell 138 (4) (2009)

709–721, https://doi.org/10.1016/j.cell.2009.05.049 (URL https://doi.org/10.1016/j.cell.2009.05.049).
[54] A. Lek, M. Lek, K.N. North, S.T. Cooper, Phylogenetic analysis of ferlin genes reveals ancient eukaryotic origins, BMC Evol. Biol. 10 (1) (2010) 231, https://doi.org/10.1186/1471-2148-10-231 (URL https://doi.org/10.1186/1471-2148-10-231).
[55] T.G.G. Battye, L. Kontogiannis, O. Johnson, H.R. Powell, A.G.W. Leslie, iMOSFLM: a new graphical interface for diffraction-image processing with mosflm, Acta Crystallogr. D Biol. Crystallogr. 67 (4) (2011) 271–281, https://doi.org/10.1107/s0907444910048675 (URL https://doi.org/10.1107/s0907444910048675).
[56] M.D. Winn, C.C. Ballard, K.D. Cowtan, E.J. Dodson, P. Emsley, P.R. Evans, R.M. Keegan, E.B. Krissinel, A.G.W. Leslie, A. McCoy, S.J. McNicholas, G.N. Murshudov, N.S. Pannu, E.A. Potterton, H.R. Powell, R.J. Read, A. Vagin, K.S. Wilson, Overview of the CCP4 suite and current developments, Acta Crystallogr. D Biol. Crystallogr. 67 (4) (2011) 235–242, https://doi.org/10.1107/s0907444910045749 (URL https://doi.org/10.1107/s0907444910045749).
[57] A.J. McCoy, R.W. Grosse-Kunstleve, P.D. Adams, M.D. Winn, L.C. Storoni, R.J. Read, Phaser crystallographic software, J. Appl. Crystallogr. 40 (Pt 4) (2007) 658–674.
[58] P.D. Adams, P.V. Afonine, G. Bunkóczi, V.B. Chen, I.W. Davis, N. Echols, J.J. Headd, L.-W. Hung, G.J. Kapral, R.W. Grosse-Kunstleve, A.J. McCoy, N.W. Moriarty, R. Oeffner, R.J. Read, D.C. Richardson, J.S. Richardson, T.C. Terwilliger, P.H. Zwart, PHENIX: a comprehensive Python-based system for macromolecular structure solution, Acta Crystallogr. D Biol. Crystallogr. 66 (2) (2010) 213–221, https://doi.org/10.1107/s0907444909052925 (URL https://doi.org/10.1107/s0907444909052925).
[59] P. Wang, C.T. Wang, J. Bai, M.B. Jackson, E.R. Chapman, Mutations in the effector binding loops in the C2A and C2B domains of synaptotagmin I disrupt exocytosis in a nonadditive manner, J. Biol. Chem. 278 (47) (2003) 47030–47037.
[60] L.L.C. Schrödinger, The PyMOL Molecular Graphics System, Version 1.8, November 2015.